Variability and trends in surface seawater pCO_2 and CO_2 flux in the Pacific Ocean

A. J. Sutton[1,2] iD, R. Wanninkhof[3] iD, C. L. Sabine[2] iD, R. A. Feely[2], M. F. Cronin[2] iD, and R. A. Weller[4] iD

[1]Joint Institute for the Study of the Atmosphere and Ocean, University of Washington, Seattle, Washington, USA, [2]Pacific Marine Environmental Laboratory, NOAA, Seattle, Washington, USA, [3]Atlantic Oceanographic and Meteorological Laboratory, NOAA, Miami, Florida, USA, [4]Woods Hole Oceanographic Institution, Woods Hole, Massachusetts, USA

Abstract Variability and change in the ocean sink of anthropogenic carbon dioxide (CO_2) have implications for future climate and ocean acidification. Measurements of surface seawater CO_2 partial pressure (pCO_2) and wind speed from moored platforms are used to calculate high-resolution CO_2 flux time series. Here we use the moored CO_2 fluxes to examine variability and its drivers over a range of time scales at four locations in the Pacific Ocean. There are significant surface seawater pCO_2, salinity, and wind speed trends in the North Pacific subtropical gyre, especially during winter and spring, which reduce CO_2 uptake over the 10 year record of this study. Starting in late 2013, elevated seawater pCO_2 values driven by warm anomalies cause this region to be a net annual CO_2 source for the first time in the observational record, demonstrating how climate forcing can influence the timing of an ocean region shift from CO_2 sink to source.

1. Introduction

The global ocean is a major sink of anthropogenic carbon dioxide (CO_2), absorbing approximately 27% of CO_2 emissions since the beginning of the industrial revolution [*Khatiwala et al.*, 2013; *Le Quéré et al.*, 2016]. Any variation or change in the ocean CO_2 sink has implications for the climate system. For example, El Niño–Southern Oscillation (ENSO) induced CO_2 flux changes in the tropical Pacific Ocean are the major source of interannual variability in the net annual global ocean CO_2 sink and results in measureable impacts on atmospheric CO_2 growth rates [*Feely et al.*, 2006; *Feely et al.*, 1999; *Rayner et al.*, 1999; *Wanninkhof et al.*, 2013]. Decadal-scale variability in the climate system has also been shown to influence CO_2 flux in the tropical Pacific [*Feely et al.*, 2006; *Ishii et al.*, 2009; *Sutton et al.*, 2014a; *Takahashi et al.*, 2003; *Wang et al.*, 2015], North Pacific [*Takahashi et al.*, 2006], North Atlantic [*McKinley et al.*, 2011], and Southern Ocean [*Landschützer et al.*, 2015]. However, there remain significant uncertainties in the magnitude of these variations in ocean CO_2 flux and even disagreements as to the direction of sea-air CO_2 flux in some regions.

A part of this uncertainty is due to insufficient observing capacity for ocean CO_2 flux over all time and space scales. Observations of ocean CO_2 flux have relied primarily on ship-based underway measurements of partial pressure of CO_2 (pCO_2). Within the last three decades, these observations have made it possible to determine seasonal to interannual variability in global ocean CO_2 flux and have contributed to a reduced uncertainty in net annual ocean CO_2 flux by 50% [*Bakker et al.*, 2016; *Landschützer et al.*, 2014; *Le Quéré et al.*, 2016; *Takahashi et al.*, 2009; *Wanninkhof et al.*, 2013].

Another contributor to uncertainty in regional and global CO_2 flux estimates is insufficient understanding of the complex and variable physical and biogeochemical processes that control CO_2 flux at subseasonal to decadal time scales. Models have been effective tools for diagnosing these drivers [*Arruda et al.*, 2015; *Frölicher et al.*, 2014; *McKinley et al.*, 2016; *Nakano et al.*, 2011; *Pilcher et al.*, 2015; *Resplandy et al.*, 2015; *Rodgers et al.*, 2014; *Wanninkhof et al.*, 2013]. However, model validation has relied primarily on a limited number of ship-based time series, and these comparisons have shown that models underestimate the seasonal cycle of surface ocean pCO_2 by about 30% in the North Atlantic, North Pacific, and Southern Ocean [*Sasse et al.*, 2015]. New autonomous measurements of ΔpCO_2 (seawater-air pCO_2) on moored platforms now allow for continuous, high-resolution observations of CO_2 flux that capture the full range of temporal variability at key locations. These CO_2 flux time series paired with additional physical and biogeochemical observations on the same platforms seek to characterize the natural and anthropogenic controls on CO_2 flux. These records of daily to decadal patterns and trends in ocean biogeochemistry can address some of these remaining

uncertainties in ocean CO_2 flux and provide expanded opportunities for validating surface ocean pCO_2 variability and change in Earth system models.

Here we calculate CO_2 flux from high-frequency mooring ΔpCO_2 and wind speed observations on four ocean reference moorings in different biomes of the Pacific Ocean: Kuroshio Extension Observatory (KEO), Ocean Station Papa, WHOI Hawaii Ocean Timeseries Station (WHOTS), and Stratus. We present the physical and biogeochemical drivers, seasonal to decadal patterns, and long-term trends in surface seawater pCO_2 and CO_2 flux.

2. Materials and Methods

2.1. Moored Locations and Carbon Measurements

Surface seawater and marine boundary layer atmospheric pCO_2 have been measured on four open ocean buoys in the Pacific since as early as 2004: Papa, KEO, WHOTS, and Stratus (Figure 1). WHOTS and Stratus are located in subtropical oligotrophic regions in the North and South Pacific, respectively. KEO is located in a region of the subtropical North Pacific with large carbon export and biological production that also experiences seasonal tropical cyclones. Papa is located in the subarctic North Pacific, another region with pronounced seasonality of physical and biological conditions. The mooring locations and time period of moored observations used in this analysis are shown in Figure 1.

A Moored Autonomous pCO_2 (MAPCO2) system is deployed on each of the four surface buoys. *Sutton et al.* [2014b] provide a full description of MAPCO2 system measurements and data processing. In brief, the MAPCO2 system utilizes an automated equilibrator-based gas collection system and an infrared gas analyzer (LI-820, LI-COR™) calibrated before, during, and after field deployment with reference gases traceable to World Meteorological Organization standards. This methodology is similar to the underway pCO_2 system deployed on a global network of ships of opportunity [*Pierrot et al.*, 2009]. The MAPCO2 system collects 3-hourly measurements of sea surface (~0.5 m depth) and marine boundary layer atmospheric (~1.5 m above sea surface) xCO_2 (the mole fraction of CO_2). Each xCO_2 measurement is paired with sea surface temperature (SST) and salinity (SSS) collected by Sea-Bird Electronics SeaCATs™. Seawater and air pCO_2 (at in situ SST) is calculated consistent with ocean CO_2 standard operating procedures [*Dickson et al.*, 2007; *Weiss*, 1974]. To adjust for the temperature effect on seawater pCO_2 (+4.23% C^{-1}), seawater pCO_2 at mean SST is also calculated using the method of *Takahashi et al.* [2002]. Overall uncertainty of the MAPCO2 is <2 µatm for seawater and <1 µatm for air pCO_2 [*Sutton et al.*, 2014b].

Seawater pCO_2, SST, and SSS measurements are also used to calculate dissolved inorganic carbon (DIC) and salinity normalized DIC (nDIC). First, total alkalinity (TA) is calculated based on the relationships with SST and/or SSS developed by *Lee et al.* [2006] for WHOTS and Stratus (uncertainty ±8 µmol kg^{-1}), by *Fassbender et al.* [2016] for Papa (uncertainty ±3 µmol kg^{-1}), and by *Fassbender et al.* [2017] for KEO (uncertainty ±6 µmol kg^{-1}). Seawater pCO_2 and TA are then used to calculate DIC in the MATLAB version (v1.1) of CO2SYS [*van Heuven et al.*, 2011] with the carbonic acid dissociation constants of *Lueker et al.* [2000], sulfate dissociation constants of *Dickson* [1990], and borate-to-salinity ratio of *Lee et al.* [2010]. DIC is then normalized to a salinity of 35: $nDIC = 35 \times DIC/SSS$.

2.2. Moored Winds and Wind Height Correction

Wind sensors are deployed on each mooring at ~3–4 m above the sea surface and measure wind speed every 1–10 min with an accuracy of 1–3% or at least 0.1 m s^{-1} [*Cronin et al.*, 2008; *Kubota et al.*, 2008; *Weller*, 2015]. Since buoy winds are only available at limited sites, CO_2 flux is commonly calculated using satellite wind products. In the supporting information we compare the Cross-Calibrated Multi-Platform (CCMP) V2.0 wind speed data with the high-quality buoy wind measurements used in this study. NCEP-DOE AMIP-II Reanalysis 2 (NCEP-2) wind speed data were also used in order to directly compare moored pCO_2 flux to the *Takahashi et al.* [2009] climatology (Figure 2c).

Wind speed is corrected to a height of 10 m above the sea surface using equation (1) derived from parameterizations of *Large and Pond* [1981]:
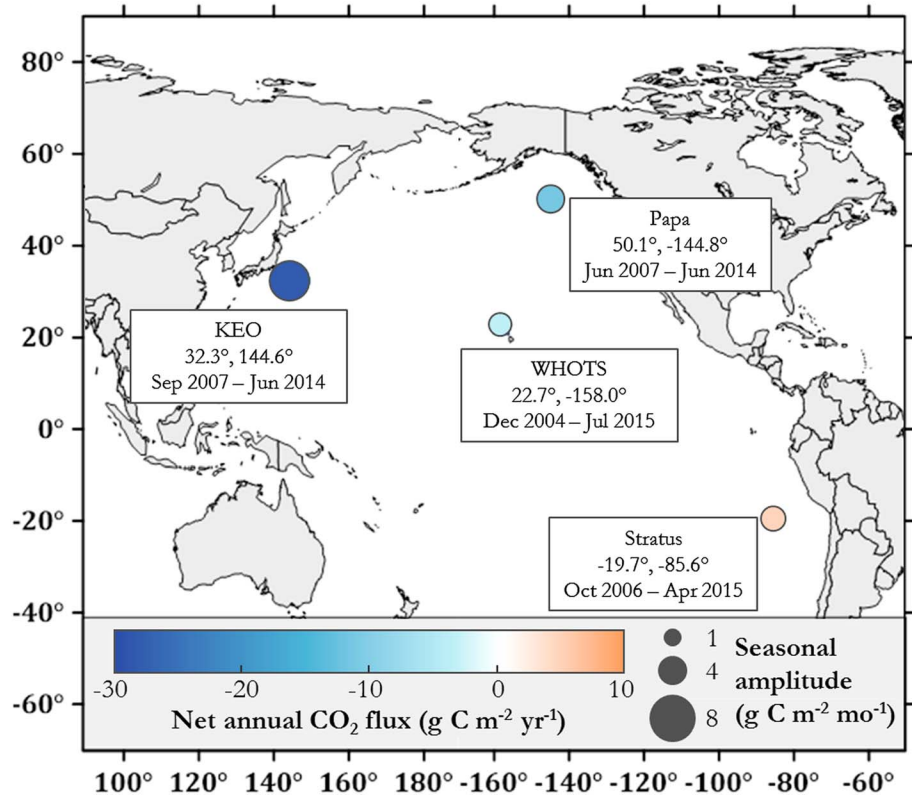
Figure 1. Net annual CO_2 flux (symbol color) and seasonal variability as measured by peak-to-peak amplitude of monthly CO_2 flux climatology (symbol size) at the Papa, KEO, WHOTS, and Stratus moorings. Here we consider the full WHOTS time series to include pCO_2 data from the Multidisciplinary Ocean Sensors for Environmental Analyses and Networks HALE-ALOHA buoy deployed December 2004 to July 2007 at 22.8°N, 158.1°W and the WHOTS buoy deployed July 2007 to present at 22.7°N, 158.0°W. Mooring abbreviation, location, and dates of time series used in the analysis are listed next to each site.

$$u10 = \frac{uZ}{1 + \frac{\sqrt{Cd10}}{0.4} \times \ln\left(\frac{Z}{10}\right)} \quad (1)$$

where $u10$ is wind speed in m s^{-1} at 10 m, Z is the height (m) of the wind sensor, uZ is wind speed in m s^{-1} recorded by the moored sensor, $Cd10$ is the drag coefficient of 0.0011, and 0.4 is von Karman's constant.

2.3. CO_2 Flux Calculation

CO_2 flux is calculated by

$$CO_2 \text{ flux} = k \times K_o \times \Delta pCO_2 \quad (2)$$

where k is the gas transfer velocity utilizing a square dependence of wind speed at 10 m, an in situ Schmidt number, and a scaling factor of 0.251 [*Wanninkhof*, 2014]; K_o is the solubility coefficient for CO_2 [*Weiss*, 1974; *Weiss et al.*, 1982]; and ΔpCO_2 is seawater pCO_2 − air pCO_2. Uncertainty of CO_2 flux calculated with moored pCO_2 and wind speed measurements is approximately 20%, which is mainly driven by the uncertainty of k [*Wanninkhof*, 2014]. The average difference between buoy wind speed measurements adjusted to 10 m using equation (1) compared to the full boundary layer stability correction in the COARE 3.0b algorithm was −0.04 ± 0.50 m s^{-1} (using Papa and KEO buoy wind time series), which does not impact total estimated CO_2 flux uncertainty.

Moored wind measurements are either provided as 2 min averages every 10 min (KEO, Papa) or 1 min measurements (WHOTS, Stratus). For calculating CO_2 flux, these winds are averaged within each 3-hourly 20 min MAPCO2 measurement cycle. CO_2 flux is presented in g C m^{-2} yr^{-1} for annual fluxes, g C m^{-2} month^{-1} for monthly flux climatologies, and g C m^{-2} h^{-1} for high-resolution moored fluxes.
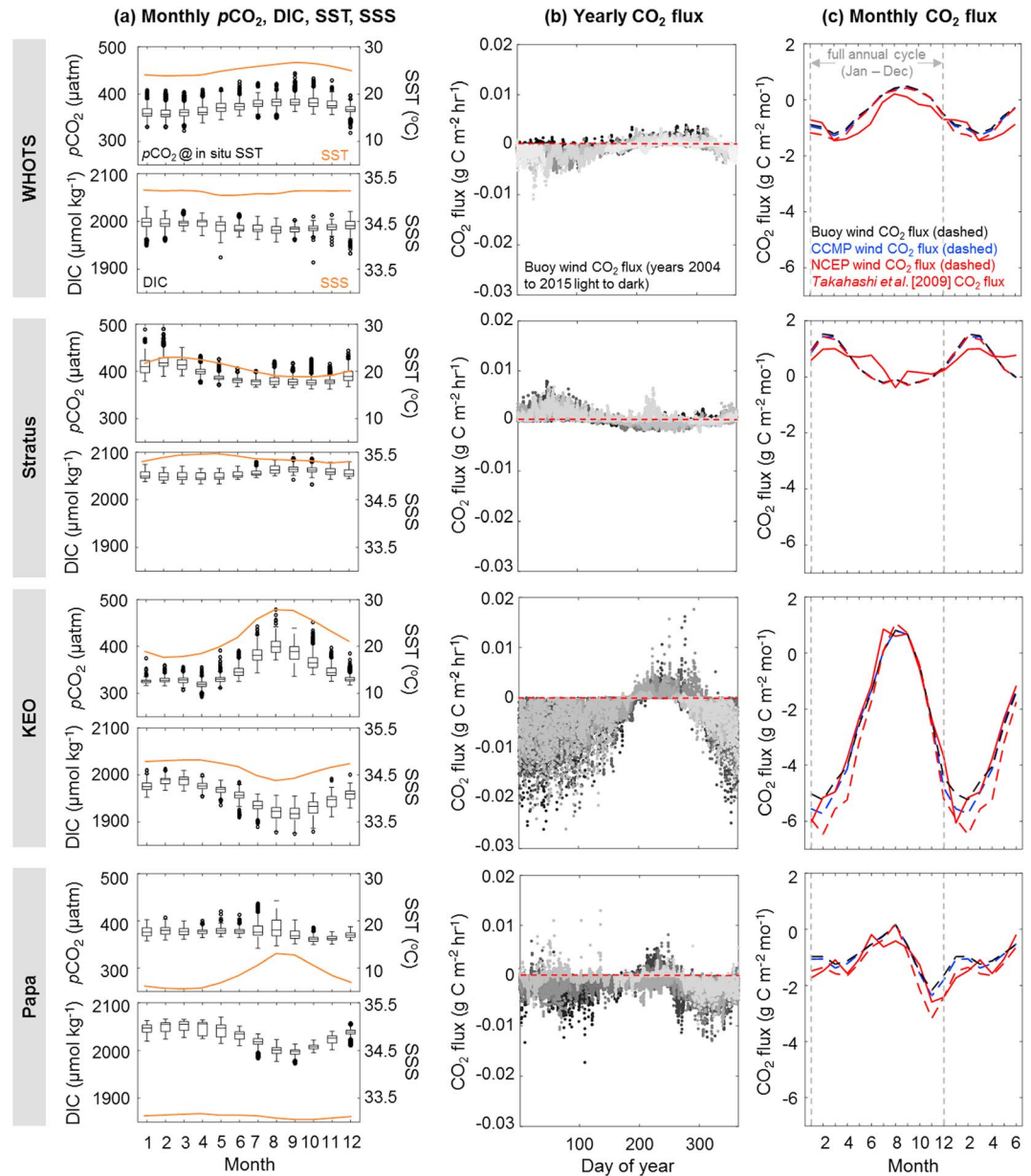
Figure 2. Seasonal and interannual variability of moored observations at WHOTS, Stratus, KEO, and Papa (rows from top to bottom). (a) Box and whisker plots (indicating the median, upper, and lower quartiles (box); 1.5 interquartile range of upper and lower quartiles (whisker); and outliers) for pCO_2 at in situ SST and DIC. Mean monthly SST and SSS values are shown in orange. (b) High-resolution CO_2 flux observations versus day of year; color scale is progressively darker from past to present starting with light gray for 2004 observations to black for 2015 observations. (c) Monthly mean CO_2 flux (with 18 month x axis to highlight the full annual cycle) using moored wind speed observations (black), CO_2 flux using CCMP wind speed (blue; see supporting information), CO_2 flux using NCEP-2 wind speed (red dashed), and data-based CO_2 flux climatologies of *Takahashi et al.* [2009] (red solid).

Net annual CO_2 flux is calculated as the sum of average monthly CO_2 fluxes over the entire mooring time series. Interannual variability is defined as 1 standard deviation (SD) of mean annual CO_2 flux using only years with a full year of moored observations, which limits the interannual comparison to only 4–5 years at each site. Seasonal variability is defined as peak-to-peak amplitude in average monthly CO_2 flux climatologies. Seasons at Papa, KEO, and WHOTS are defined as winter = December–February; spring = March–May; summer = June–August; fall = September–November. Seasons are the opposite at Stratus.

3. Results and Discussion

3.1. Processes Driving Seasonal Variability

At the WHOTS mooring in the North Pacific subtropical gyre, surface seawater pCO_2 follows the same seasonal pattern as SST with higher values in summer and lower values in winter (Figure 2a). This seasonal pattern is opposite for DIC and pCO_2 at mean SST with biological activity decreasing DIC in summer and winter mixing bringing deep water high in DIC to the surface (Figure 2a). Wind speed is relatively constant throughout the year but with higher variability during winter (Figure S1 in the supporting information). The WHOTS location is generally a CO_2 sink from December to June and a source from July to October (Figures 2b and 2c).

In the South Pacific subtropics, Stratus follows similar seasonal patterns as WHOTS with a few exceptions. SST is lower and seawater pCO_2 and DIC values are higher (Figure 2a). Monthly variability is higher year round for SST and DIC at Stratus compared to WHOTS. This is also the case for pCO_2 but only during the high pCO_2 period during summer months. The Stratus site is generally a CO_2 source from December to May and a sink from July to November (Figures 2b and 2c).

At the KEO mooring in the Kuroshio Extension Current, seawater pCO_2 also follows the same seasonal pattern as SST with higher values in summer and lower values in winter, while summer biological production and winter mixing likely contribute to the opposite pattern for DIC and pCO_2 at mean SST (Figure 2a). Seasonal patterns of DIC and SSS are similar at KEO, highlighting the influence of seasonal evaporation and precipitation on sea surface DIC in this region (Figure 2a). A mixed layer budget developed at KEO also reveals these seasonal patterns [*Fassbender et al.*, 2017]. Although wind speed at KEO follows the same seasonal patterns as WHOTS and Stratus, wind speeds are higher and more variable through the entire year compared to the other subtropical sites (Figure S1). This higher wind speed contributes to the KEO region being a strong CO_2 sink throughout most of the year (Figures 2b and 2c).

In the subarctic North Pacific at Papa, opposing strong influences of SST and DIC seasonality cause less seasonal variation in seawater pCO_2 compared to the other sites (Figure 2a). Previous studies have found a strong biological pump at Ocean Station Papa with significant seasonality in net community production [*Emerson et al.*, 2011; *Fassbender et al.*, 2016]. Net community production can be highly variable during the late winter to early spring transitions when the surface ocean oscillates between shallow thermal stratification and storm-induced mixed layer deepening (Figure 2b). This study also confirms that Papa is a CO_2 sink throughout most of the year (Figures 2b and 2c) with wind speed values and seasonality similar to the KEO location (Figure S1).

The seasonal range of surface seawater pCO_2 at mean SST and DIC are higher at KEO and Papa compared to WHOTS and Stratus (Figure 2a). Similar patterns between sites were found in observations of sea surface pH and aragonite saturation state [*Sutton et al.*, 2016]. This difference is attributed to larger seasonality of SST and productivity compared to the oligotrophic subtropical waters where WHOTS and Stratus reside. Consistent trade winds and shallow mixed layer depth throughout the year at WHOTS and Stratus are also characteristic of weaker physical forcing of biogeochemical variability. This is in contrast to Papa and KEO, where biogeochemical variability is influenced by deep winter convection and high frequency of winter storms and typhoons.

Correlation coefficients testing the relationship between parameters support these observed seasonal patterns and drivers (Table S1). WHOTS and Stratus show similar relationships, with seawater pCO_2 most strongly correlated with SST, and CO_2 flux most strongly correlated with ΔpCO_2. Higher biological activity and strong seasonality in upper ocean physical forcing likely cause seawater pCO_2 at KEO to be strongly correlated with not only SST but also SSS and nDIC. CO_2 flux at KEO and Papa is strongly correlated to both ΔpCO_2 and wind speed, with higher wind speed driving stronger CO_2 uptake (i.e., negative correlation). In terms of seawater pCO_2, Papa is a clear anomaly compared to the other three locations, and simple two-parameter correlations do not capture the more complicated biogeochemical drivers at this location.

3.2. Net Annual Flux: Mooring Versus Data-Based Products and Models

Net annual CO_2 flux over the moored time series indicates that the KEO location has the strongest CO_2 sink (-28.5 g C m^{-2} yr^{-1}), with less uptake at Papa (-11.7 g C m^{-2} yr^{-1}) and WHOTS (-3.9 g C m^{-2} yr^{-1}). With a net annual CO_2 flux of 4.7 g C m^{-2} yr^{-1}, Stratus is the only location in this study that is a net CO_2 source to the
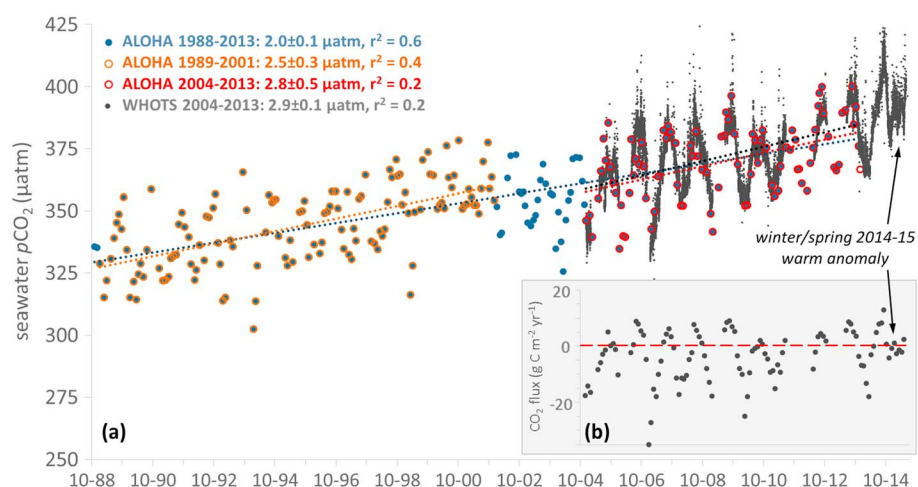
Figure 3. (a) Surface seawater pCO$_2$ time series from station ALOHA 1988–2013 (blue), ALOHA 1989–2001 (orange-outlined circles), ALOHA 2004–2014 (red-outlined circles), and WHOTS 2004–2015 (black) with trend lines in same colors (observations after 13 November are not included in WHOTS trend analysis). Observations used in the trends shown here are not deseasoned. Dates are MM-YY. (b) Monthly CO$_2$ flux observations at WHOTS 2004–2015. Time axis corresponds to time axis in Figure 3a.

atmosphere (Figures 1 and 3). In general, CO$_2$ flux seasonality at all locations (Figure 2c) follows patterns of seawater pCO$_2$ and SST (Figure 2a) with periods of CO$_2$ outgassing during summer and CO$_2$ uptake during winter. Seasonal variability, as measured by peak-to-peak amplitude in the seasonal cycle is the same at WHOTS and Stratus (1.7 g C m^{-2} month^{-1}), slightly higher at Papa (2.3 g C m^{-2} month^{-1}), and the highest at KEO (6.0 g C m^{-2} month^{-1}; Figure 1). Interannual variability is approximately 2 g C m^{-2} yr^{-1} at WHOTS, Stratus, and KEO and only 1 g C m^{-2} yr^{-1} at Papa; however, these estimates are based on comparisons of only 4–5 years at each site, so much longer time series are necessary to confirm the interannual patterns.

In general, monthly climatologies of moored CO$_2$ flux are similar to climatologies of ship-based CO$_2$ flux (Figure 2c) [*Takahashi et al.*, 2009]. Some discrepancies include the following: WHOTS mooring CO$_2$ flux is on average 60% higher throughout the year, Stratus mooring CO$_2$ flux exhibits a more pronounced seasonal trend with a 26% higher seasonal amplitude, and, in general, winter CO$_2$ flux estimated from the Papa mooring time series is on average 44% higher in the winter compared to the *Takahashi et al.* [2009] climatologies. The main sources of these discrepancies are likely the lack of full seasonal coverage from ship-based data, a different treatment of the gas exchange wind speed relationship, and the use of different wind speed data (*Takahashi et al.* [2009] uses NCEP-2 wind speed data). The largest discrepancies between CO$_2$ flux estimates based on different wind speed data are during the winter season at Papa and KEO (Figure 2c).

In a recent global analysis of various data-based estimates of CO$_2$ flux, net annual CO$_2$ flux estimates by *Rödenbeck et al.* [2015] in the ocean biome regions (as defined by *Fay and McKinley* [2013]) where WHOTS, KEO, and Papa moorings reside are roughly equivalent to CO$_2$ flux calculated from the mooring observations. However, within the region where Stratus resides (i.e., South Pacific subtropical permanently stratified biome), the *Rödenbeck et al.* [2015] average surface seawater pCO$_2$ observations are about 10% lower than pCO$_2$ observed at Stratus (Figure 2a). As a result, all the various approaches synthesized by *Rödenbeck et al.* [2015] suggest that this region is a net sink, whereas the mooring observations show that the Stratus location is a net annual CO$_2$ source (Figures 1 and 2). One explanation for this discrepancy is that the extremely limited ship-based data in this region are not sufficient to constrain net annual CO$_2$ flux. It is also possible that the Stratus mooring location is not representative of mean conditions in the South Pacific subtropical permanently stratified biome. The moored location may be influenced by DIC-rich water upwelled along the South American coast, elevating seawater pCO$_2$ at this particular location, which would not influence the majority of this biome region farther from the coast. In contrast, the WHOTS, KEO, and Papa locations seem to be representative of CO$_2$ flux conditions within the biomes they reside [*Rödenbeck et al.*, 2015].

3.3. Mooring Time Series Trends

Deseasoned seawater pCO_2 trends are statistically significant at all sites (Table S2). Linear trends over the period of each moored time series are presented in Table S2. However, model estimations of trend detection times [*Keller et al.*, 2014; *Lovenduski et al.*, 2015] suggest that trends in surface seawater pCO_2 and pH attributable to long-term anthropogenic change do not emerge from natural variability before an approximately 15 year observation record at Stratus and a 10 year record at KEO and Papa, which are longer than the length of the existing moored time series at these locations (Figure 1). Moored wind speed observations and CO_2 flux trends over the full pCO_2 time series were not significant at any mooring location, which is consistent with modeling results of *McKinley et al.* [2016] suggesting anthropogenic trends of CO_2 flux do not emerge from natural variability until as early as a 30 year time series in the least variable regions.

Even though we cannot yet detect an anthropogenic trend over natural variability at these three sites, the moored time series provide insight into potential processes driving interannual to decadal patterns in these regions. For example, a significant increase in trade winds at Stratus of 15% was observed between 2000 and 2009 [*Weller*, 2015] and assuming no significant change in ΔpCO_2 (Table S2), winds alone during that time period would account for an intensification of CO_2 outgassing of 28%. In addition, between 2007 and 2014 Ocean Station Papa has shown unique seasonal (Figure 2) and long-term (Table S2) patterns compared to the other mooring locations. At Papa, SST is warming and both ΔpCO_2 and nDIC are decreasing. Long-term observations will be necessary to track whether this trend continues and results in a weakening of the CO_2 sink at this location. Because continued ocean acidification is projected to reduce the role calcifiers play in carbon export, which is potentially very large at Papa [*Fassbender et al.*, 2016], these observations are critical to track and diagnose the controls of ocean carbon uptake in the long term.

3.3.1. WHOTS and Station ALOHA

The modeling results of *Keller et al.* [2014] and *Lovenduski et al.* [2015] do suggest that the WHOTS mooring time series is long enough to detect a trend over natural variability in pCO_2 and pH (trend detection time ~10 years). Here we observe a significant trend in deseasoned seawater pCO_2 of 3.4 ± 0.2 µatm yr^{-1} from 2004 to 2015.

North Pacific warm anomalies beginning in winter 2013–2014 [*Bond et al.*, 2015] intensify the upward seawater pCO_2 trend (Figure 3). The trend in deseasoned seawater pCO_2 at WHOTS excluding observations from winter 2013 to the end of the time series is 1 µatm yr^{-1} less than when those observations are included in the trend analysis. Observations toward the end of the WHOTS time series suggest that elevated seawater pCO_2 values largely driven by North Pacific warm anomalies led the WHOTS site to be a net annual CO_2 source from mid-2014 to mid-2015 for the first time in the moored pCO_2 record (Figure 3b). Due to this anomalous event, seawater observations from December 2013 to the end of the time series are excluded from the remainder of the long-term trend analyses. Resulting trends in deseasoned seawater pCO_2 and pH from 2004 to 2013 are 2.4 ± 0.2 µatm yr^{-1} and -0.002 ± 0.0003, respectively (Table S2), which are the rates expected from seawater equilibration with rising atmospheric pCO_2.

While seawater pCO_2 is primarily driven by SST on a seasonal and interannual basis, the lack of a significant trend in deseasoned SST from 2004 to 2013 (Table S2) suggests that an ocean warming trend is not influencing the pCO_2 trend. Some of the processes driving pCO_2 trends do emerge when investigating deseasoned observations in each of the four seasons separately. Seawater pCO_2 trends are higher in winter/spring (3.0 ± 0.8 µatm yr^{-1}, $r^2 = 0.5$) versus summer/fall (2.3 ± 0.4 µatm yr^{-1}, $r^2 = 0.5$). There is also a significant trend in SSS (0.02 ± 0.01 yr^{-1}; $r^2 = 0.2$), which is driven by higher rates of change in winter (0.06 ± 0.01 yr^{-1}; $r^2 = 0.5$) and may indicate reduced rainfall and enhanced evaporation at this location during the winter season [*Dore et al.*, 2003; *Lukas and Santiago-Mandujano*, 2008]. Over the time series, this salinity change only accounts for a small portion (<5%) of the observed seawater pCO_2 increase due to the impact that salinity has on pCO_2 [*Weiss et al.*, 1982] but does indicate physical changes in the subtropical North Pacific that may influence ocean biogeochemistry.

Wind speed trends also vary by season with strong negative trends for the summer, fall, and winter seasons (-0.13 ± 0.05 m s^{-1} yr^{-1}, $r^2 = 0.2$). Although there is no trend in CO_2 flux over the full WHOTS time series, seasonal wind speed and seawater pCO_2 trends contribute to significant long-term trends in CO_2 flux during winter (0.4 ± 0.1 g C m^{-2} yr^{-1}, $r^2 = 0.4$) and spring (0.2 ± 0.1 g C m^{-2} yr^{-1}, $r^2 = 0.3$); there are no significant

CO_2 flux trends in summer and fall. These winter and spring flux trends suggest that the WHOTS site will go from being a net annual sink to a net annual source by the year 2040 if current long-term trends in wind and pCO_2 prevail. However, it is clear that North Pacific warm anomalies in 2013–2015 are an example of interannual physical forcing that already tipped this location from being a sink to a source, well before 2040 (Figure 3). Continued observations at this site will be necessary to fully resolve how these types of ephemeral events impact the long-term trends projected for this site.

Extending the time series with ship-based observations also show how natural variability impacts CO_2 flux predictions. Based on ΔpCO_2 trends observed at station ALOHA from 1989 to 2001, *Dore et al.* [2003] predicted faster rates of change in CO_2 flux with a shift from net annual sink to source occurring in 2008. However, the strong surface seawater pCO_2 trends of 2.5 ± 0.3 μatm yr^{-1} observed by *Dore et al.* [2003] during the 1989–2001 time frame that were driving ΔpCO_2 trends were likely influenced by interannual and/or decadal variations. Between the *Dore et al.* [2003] analysis (ending in 2001) and the start of the WHOTS mooring time series (beginning December 2004), there was no significant trend; however, the rapid rate of change resumes post-WHOTS pCO_2 deployment (Figure 3). With a trend uncertainty of approximately ± 0.3 μatm yr^{-1}, the seawater pCO_2 trend reported for the 1989–2001 station ALOHA time series [*Dore et al.*, 2003] as well as the ALOHA and WHOTS trends since 2004 are similar. The station ALOHA time series (not deseasoned) over the full 25 year record has a long-term trend of 2.0 ± 0.1 μatm yr^{-1}, which is significantly different from the two intervals of more rapid rates of change (Figure 3).

The impact of the North Pacific warm anomaly and the variability in station ALOHA and WHOTS time series trends illustrate significant interannual to decadal variability in seawater pCO_2 and CO_2 flux. The physical climate forcings that likely contribute to this interannual to decadal variability at WHOTS include variations in winter freshwater input, wind stress, and other large-scale processes connecting the subtropical North Pacific to other regions of the Pacific [*Lukas and Santiago-Mandujano*, 2008; *Stammer et al.*, 2008]. This variability suggests that contrary to the modeling results of *Keller et al.* [2014], 10 years may not be enough time to define the long-term anthropogenic trend in seawater pCO_2 in this region.

4. Conclusions

Seasonally constrained observations collected continuously over a long time period improve the ability to diagnose trends and drivers of sea-air CO_2 flux. Using the approach of colocated moored observations of sea surface pCO_2 and physical conditions, we discover that predicting when the subtropical North Pacific gyre region will transition from CO_2 sink to source cannot be done without investigating the patterns within each season separately. In this case, significant seawater pCO_2, SSS, and wind speed trends occur during winter and spring, a finding that may go undetected if only using ship measurements with limited winter occupations. In addition, we find that even in this low-variability oligotrophic region, interannual to decadal changes influence seawater pCO_2 trends within a 10 year window, which suggests that the model-predicted trend detection time of 10 years may not be sufficient to define the long-term anthropogenic signature. The eventual shift from CO_2 sink to source will depend not only on anthropogenic change but also on how climatic oscillations, such as the Pacific Decadal Oscillation and North Pacific Gyre Oscillation, influence this region into the future. Anomalous North Pacific warming in 2013–2015 may be the first example of a climatic driver that starts to force this region from a CO_2 sink to a source.

References

Arruda, R., P. H. R. Calil, A. A. Bianchi, S. C. Doney, N. Gruber, I. Lima, and G. Turi (2015), Air-sea CO_2 fluxes and the controls on ocean surface pCO_2 seasonal variability in the coastal and open-ocean southwestern Atlantic Ocean: A modeling study, *Biogeosciences*, *12*(19), 5793–5809, doi:10.5194/bg-12-5793-2015.

Bakker, D. C. E., et al. (2016), A multi-decade record of high-quality fCO_2 data in version 3 of the Surface Ocean CO_2 Atlas (SOCAT), *Earth Syst. Sci. Data*, *8*(2), 383–413, doi:10.5194/essd-8-383-2016.

Bond, N. A., M. F. Cronin, H. Freeland, and N. Mantua (2015), Causes and impacts of the 2014 warm anomaly in the NE Pacific, *Geophys. Res. Lett.*, *42*, 3414–3420, doi:10.1002/2015GL063306.

Cronin, M. F., C. Meinig, C. L. Sabine, H. Ichikawa, and H. Tomita (2008), Surface mooring network in the Kuroshio Extension, *IEEE Syst. Spec. Issue GEOSS*, *2*(3), 424–430, doi:10.1109/JSYST.2008.925982.

Dickson, A. G. (1990), Standard potential of the reaction: AgCl(s) + 1/2 H$_2$(g) = Ag(s) + HCl(aq), and the standard acidity constant of the ion HSO$_4^-$ in synthetic sea water from 273.15 to 318.15 K, *J. Chem. Thermodyn.*, *22*, 113–127.

Dickson, A. G., C. L. Sabine, and J. R. Christian (Eds.) (2007), *Guide to Best Practices for Ocean CO_2 Measurements*, 176 pp., North Pacific Marine Science Organization. [Available at http://cdiac.ornl.gov/oceans/Handbook_2007.html.]

Dore, J. E., R. Lukas, D. W. Sadler, M. J. Church, and D. M. Karl (2009), Physical and biogeochemical modulation of ocean acidification in the central North Pacific, *Proc. Natl. Acad. Sci. U.S.A.*, *106*(30), 12,235–12,240, doi:10.1073/pnas.0906044106.

Dore, J. E., R. Lukas, D. W. Sadler, and D. M. Karl (2003), Climate-driven changes to the atmospheric CO_2 sink in the subtropical North Pacific Ocean, *Nature*, *424*(6950), 754–757.

Emerson, S., C. Sabine, M. F. Cronin, R. Feely, S. E. Cullison Gray, and M. DeGrandpre (2011), Quantifying the flux of $CaCO_3$ and organic carbon from the surface ocean using in situ measurements of O_2, N_2, pCO_2, and pH, *Global Biogeochem. Cycles*, *25*, GB3008, doi:10.1029/2010GB003924.

Fassbender, A. J., C. L. Sabine, and M. F. Cronin (2016), Net community production and calcification from seven years of NOAA Station Papa Mooring measurements, *Global Biogeochem. Cycles*, *31*, 250–267, doi:10.1002/2015GB005205.

Fassbender, A. J., C. L. Sabine, M. F. Cronin, and A. J. Sutton (2017), Mixed-layer carbon cycling at the Kuroshio Extension Observatory, *Global Biogeochem. Cycles*, doi:10.1002/2016GB005547.

Fay, A. R., and G. A. McKinley (2013), Global trends in surface ocean pCO_2 from in situ data, *Global Biogeochem. Cycles*, *27*, 541–557, doi:10.1002/gbc.20051.

Feely, R. A., T. Takahashi, R. Wanninkhof, M. J. McPhaden, C. E. Cosca, S. C. Sutherland, and M.-E. Carr (2006), Decadal variability of the air-sea CO_2 fluxes in the equatorial Pacific Ocean, *J. Geophys. Res.*, *111*, C08S90, doi:10.1029/2005JC003129.

Feely, R. A., R. Wanninkhof, T. Takahashi, and P. Tans (1999), Influence of El Niño on the equatorial Pacific contribution to atmospheric CO_2 accumulation, *Nature*, *398*(6728), 597–601.

Frölicher, T. L., J. L. Sarmiento, D. J. Paynter, J. P. Dunne, J. P. Krasting, and M. Winton (2014), Dominance of the Southern Ocean in anthropogenic carbon and heat uptake in CMIP5 models, *J. Clim.*, *28*(2), 862–886, doi:10.1175/JCLI-D-14-00117.1.

Ishii, M., et al. (2009), Spatial variability and decadal trend of the oceanic CO_2 in the western equatorial Pacific warm/fresh water, *Deep Sea Res., Part II*, *56*(8–10), 591–606, doi:10.1016/j.dsr2.2009.01.002.

Keller, K. M., F. Joos, and C. C. Raible (2014), Time of emergence of trends in ocean biogeochemistry, *Biogeosciences*, *11*(13), 3647–3659, doi:10.5194/bg-11-3647-2014.

Khatiwala, S., et al. (2013), Global ocean storage of anthropogenic carbon, *Biogeosciences*, *10*, 2169–2191, doi:10.5194/bg-10-2169-2013.

Kubota, M., N. Iwabe, M. F. Cronin, and H. Tomita (2008), Surface heat fluxes from the NCEP/NCAR and NCEP/DOE reanalyses at the KEO buoy site, *J. Geophys. Res.*, *113*, C02009, doi:10.1029/2007JC004338.

Landschützer, P., N. Gruber, D. C. E. Bakker, and U. Schuster (2014), Recent variability of the global ocean carbon sink, *Global Biogeochem. Cycles*, *30*, 927–949, doi:10.1002/2014GB004853.

Landschützer, P., et al. (2015), The reinvigoration of the Southern Ocean carbon sink, *Science*, *349*(6253), 1221–1224, doi:10.1126/science.aab2620.

Large, W. G., and S. Pond (1981), Open ocean momentum flux measurements in moderate to strong winds, *J. Phys. Oceanogr.*, *11*(3), 324–336, doi:10.1175/1520-0485(1981)011<0324:oomfmi>2.0.co;2.

Le Quéré, C., et al. (2016), Global carbon budget 2016, *Earth Syst. Sci. Data*, *8*(2), 605–649, doi:10.5194/essd-8-605-2016.

Lee, K., T.-W. Kim, R. H. Byrne, F. J. Millero, R. A. Feely, and Y.-M. Liu (2010), The universal ratio of boron to chlorinity for the North Pacific and North Atlantic Oceans, *Geochim. Cosmochim. Acta*, *74*(6), 1801–1811, doi:10.1016/j.gca.2009.12.027.

Lee, K., L. T. Tong, F. J. Millero, C. L. Sabine, A. G. Dickson, C. Goyet, G.-H. Park, R. Wanninkhof, R. A. Feely, and R. M. Key (2006), Global relationships of total alkalinity with salinity and temperature in surface waters of the world's oceans, *Geophys. Res. Lett.*, *33*, L19605, doi:10.1029/2006GL027207.

Lovenduski, N. S., M. C. Long, and K. Lindsay (2015), Natural variability in the surface ocean carbonate ion concentration, *Biogeosciences*, *12*(21), 6321–6335, doi:10.5194/bg-12-6321-2015.

Lueker, T. J., A. G. Dickson, and C. D. Keeling (2000), Ocean pCO_2 calculated from dissolved inorganic carbon, alkalinity, and equations for K1 and K2: Validation based on laboratory measurements of CO_2 in gas and seawater at equilibrium, *Mar. Chem.*, *70*(1–3), 105–119, doi:10.1016/S0304-4203(00)00022-0.

Lukas, R., and F. Santiago-Mandujano (2008), Interannual to interdecadal salinity variations observed near Hawaii: Local and remote forcing by surface freshwater fluxes, *Oceanography*, *21*(1), 46–55.

McKinley, G. A., A. R. Fay, T. Takahashi, and N. Metzl (2011), Convergence of atmospheric and North Atlantic carbon dioxide trends on multidecadal timescales, *Nat. Geosci.*, *4*, 606–610, doi:10.1038/ngeo1193.

McKinley, G. A., D. J. Pilcher, A. R. Fay, K. Lindsay, M. C. Long, and N. S. Lovenduski (2016), Timescales for detection of trends in the ocean carbon sink, *Nature*, *530*(7591), 469–472, doi:10.1038/nature16958.

Nakano, H., H. Tsujino, M. Hirabara, T. Yasuda, T. Motoi, M. Ishii, and G. Yamanaka (2011), Uptake mechanism of anthropogenic CO_2 in the Kuroshio Extension region in an ocean general circulation model, *J. Oceanogr.*, *67*(6), 765–783, doi:10.1007/s10872-011-0075-7.

Pierrot, D., C. Neill, K. Sullivan, R. Castle, R. Wanninkhof, H. Lüger, T. Johannessen, A. Olsen, R. A. Feely, and C. E. Cosca (2009), Recommendations for autonomous underway pCO_2 measuring systems and data-reduction routines, *Deep Sea Res., Part II*, *56*(8–10), 512–522, doi:10.1016/j.dsr2.2008.12.005.

Pilcher, D. J., S. R. Brody, L. Johnson, and B. Bronselaer (2015), Assessing the abilities of CMIP5 models to represent the seasonal cycle of surface ocean pCO_2, *J. Geophys. Res. Oceans*, *120*, 4625–4637, doi:10.1002/2015JC010759.

Rayner, P. J., R. M. Law, and R. Dargaville (1999), The relationship between tropical CO_2 fluxes and the El Niño–Southern Oscillation, *Geophys. Res. Lett.*, *26*(4), 493–496, doi:10.1029/1999GL900008.

Resplandy, L., R. Séférian, and L. Bopp (2015), Natural variability of CO_2 and O_2 fluxes: What can we learn from centuries-long climate models simulations?, *J. Geophys. Res. Oceans*, *120*, 384–404, doi:10.1002/2014JC010463.

Rödenbeck, C., et al. (2015), Data-based estimates of the ocean carbon sink variability—First results of the Surface Ocean pCO_2 Mapping intercomparison (SOCOM), *Biogeosci. Discuss.*, *12*(16), 14,049–14,104, doi:10.5194/bgd-12-14049-2015.

Rodgers, K. B., O. Aumont, S. E. Mikaloff Fletcher, Y. Plancherel, L. Bopp, C. de Boyer Montégut, D. Iudicone, R. F. Keeling, G. Madec, and R. Wanninkhof (2014), Strong sensitivity of Southern Ocean carbon uptake and nutrient cycling to wind stirring, *Biogeosciences*, *11*(15), 4077–4098, doi:10.5194/bg-11-4077-2014.

Sasse, T. P., B. I. McNeil, R. J. Matear, and A. Lenton (2015), Quantifying the influence of CO_2 seasonality on future aragonite undersaturation onset, *Biogeosciences*, *12*(20), 6017–6031, doi:10.5194/bg-12-6017-2015.

Stammer, D., S. Park, A. Köhl, R. Lukas, and F. Santiago-Mandujano (2008), Causes for large-scale hydrographic changes at the Hawaii Ocean Time series station, *J. Phys. Oceanogr.*, *38*(9), 1931–1948, doi:10.1175/2008JPO3751.1.

Sutton, A. J., R. A. Feely, C. L. Sabine, M. J. McPhaden, T. Takahashi, F. P. Chavez, G. E. Friederich, and J. T. Mathis (2014a), Natural variability and anthropogenic change in equatorial Pacific surface ocean pCO_2 and pH, *Global Biogeochem. Cycles*, *28*, 131–145, doi:10.1002/2013GB00467.

Sutton, A. J., et al. (2014b), A high-frequency atmospheric and seawater pCO$_2$ data set from 14 open-ocean sites using a moored autonomous system, *Earth Syst. Sci. Data*, *6*(2), 353–366, doi:10.5194/essd-6-353-2014.

Sutton, A. J., et al. (2016), Using present-day observations to detect when anthropogenic change forces surface ocean carbonate chemistry outside preindustrial bounds, *Biogeosciences*, *13*(17), 5065–5083, doi:10.5194/bg-13-5065-2016.

Takahashi, T., S. C. Sutherland, R. A. Feely, and C. E. Cosca (2003), Decadal variation of the surface water PCO$_2$ in the western and central equatorial Pacific, *Science*, *302*(5646), 852–856, doi:10.1126/science.1088570.

Takahashi, T., S. C. Sutherland, R. A. Feely, and R. Wanninkhof (2006), Decadal change of the surface water pCO$_2$ in the North Pacific: A synthesis of 35 years of observations, *J. Geophys. Res.*, *111*, C07S05, doi:10.1029/2005JC003074.

Takahashi, T., et al. (2002), Global sea-air CO$_2$ flux based on climatological surface ocean pCO$_2$, and seasonal biological and temperature effects, *Deep Sea Res., Part II*, *49*(9–10), 1601–1622, doi:10.1016/S0967-0645(02)00003-6.

Takahashi, T., et al. (2009), Climatological mean and decadal change in surface ocean pCO$_2$, and net sea-air CO$_2$ flux over the global oceans, *Deep Sea Res., Part II*, *56*(8–10), 554–577, doi:10.1016/j.dsr2.2008.12.009.

van Heuven, S., D. Pierrot, J. W. B. Rae, E. Lewis, and D. W. R. Wallace (2011), MATLAB program developed for CO$_2$ system calculations, ORNL/CDIAC-105b, Carbon Dioxide Inf. Anal. Cent., Oak Ridge Natl. Lab., US DOE, Oak Ridge, Tenn.

Wang, X., R. Murtugudde, E. Hackert, J. Wang, and J. Beauchamp (2015), Seasonal to decadal variations of sea surface pCO$_2$ and sea-air CO$_2$ flux in the equatorial oceans over 1984–2013: A basin-scale comparison of the Pacific and Atlantic Oceans, *Global Biogeochem. Cycles*, *29*, 597–609, doi:10.1002/2014GB005031.

Wanninkhof, R. (2014), Relationship between wind speed and gas exchange over the ocean revisited, *Limnol. Oceanogr. Methods*, *12*(6), 351–362, doi:10.4319/lom.2014.12.351.

Wanninkhof, R., et al. (2013), Global ocean carbon uptake: Magnitude, variability and trends, *Biogeosci. Discuss.*, *9*(8), 10,961–11,012, doi:10.5194/bgd-9-10961-2012.

Weiss, R. F. (1974), Carbon dioxide in water and seawater: The solubility of a non-ideal gas, *Mar. Chem.*, *2*(3), 203–215, doi:10.1016/0304-4203(74)90015-2.

Weiss, R. F., R. A. Jahnke, and C. D. Keeling (1982), Seasonal effects of temperature and salinity on the partial pressure of CO$_2$ in seawater, *Nature*, *300*(5892), 511–513.

Weller, R. A. (2015), Variability and trends in surface meteorology and air–sea fluxes at a site off northern Chile, *J. Clim.*, *28*(8), 3004–3023, doi:10.1175/JCLI-D-14-00591.1.